

Magnetically generated spin-orbit coupling for ultracold atoms with slowly varying periodic drivingD. Burba¹, M. Mackoīt-Sinkevičienė¹, V. Novičenko¹, E. Witkowska² and G. Juzeliūnas¹¹*Institute of Theoretical Physics and Astronomy, Vilnius University, Saulėtekio 3, 10257 Vilnius, Lithuania*²*Institute of Physics PAS, Aleja Lotnikow 32/46, 02-668 Warszawa, Poland*

(Received 28 September 2023; revised 9 May 2024; accepted 13 May 2024; published 30 May 2024)

The spin-orbit coupling (SOC) affecting the center of mass of ultracold atoms can be simulated using a properly chosen periodic sequence of magnetic pulses. Yet such a method is generally accompanied by micromotion, which hinders precise control of atomic dynamics, thus complicating practical applications. Here we show how to bypass the micromotion emerging in the magnetically induced SOC by properly switching on and off the oscillating magnetic fields at the initial and final times. We consider the exact dynamics of the system and demonstrate that the overall dynamics can be immune to the micromotion. The exact dynamics is shown to agree well with the evolution of the system described by the slowly changing effective Floquet Hamiltonian including the SOC term. The agreement is shown to be best when the phase of the periodic driving takes a specific value for which the effect of the spin-orbit coupling is maximum.

DOI: [10.1103/PhysRevA.109.053319](https://doi.org/10.1103/PhysRevA.109.053319)**I. INTRODUCTION**

Spin-orbit coupling (SOC) manifests for electrons in solids [1], where manipulation of electron spins by SOC plays an important role in spintronics and quantum information processing. During the past decade there has been also a great deal of interest in SOC for ultracold atoms [2–9]. The SOC can lead to novel many-body phases for ultracold atoms [6–8] and offers applications in areas such as spintronics [10,11] and precision measurements [12,13].

The SOC affecting the center of mass of ultracold atoms is usually created by applying laser fields which induce transitions between the atomic internal states accompanied by the recoil [2–8]. This provides an effective coupling between the atomic spin and linear momentum. Alternatively, the SOC can be simulated by means of a properly chosen periodic sequence of magnetic pulses [14,15], a method that has been implemented for rubidium and sodium atoms [16,17]. Specifically, by applying to ultracold atoms an oscillating magnetic field with a spatial gradient and an additional pulsed magnetic field, one can simulate an effective spin-orbit coupling similar to the one induced by laser fields. The magnetic-based approach can provide fast and flexible changes of the system parameters, such as the recoil momentum. This can be useful for controlling and manipulating atomic spin states.

The SOC created by the oscillating magnetic field is generally accompanied by micromotion, which hinders precise control of atomic dynamics and thus complicates applications. These include a fundamental study of the generation of topological states [6,18,19], subwavelength lattices [20,21], and nontrivial quantum correlations like spin squeezing [12,13,22] or indirectly Bell correlations [23].

Here we show how to bypass the micromotion emerging in the magnetically induced SOC by switching on and off properly the oscillating magnetic fields at the initial and final times. We consider the exact dynamics of the system from the initial to the final times and demonstrate that the overall dynamics

can be immune to the micromotion. Furthermore, the exact dynamics agrees well with the evolution of the system described by the slowly changing effective Floquet Hamiltonian which contains the SOC term. The agreement is best when the phase of the periodic driving takes a specific value for which the effect of the spin-orbit coupling is maximum. In that case, the first-order effective Floquet Hamiltonian vanishes and the zeroth-order Floquet Hamiltonian is correct up to the second-order expansion in the inverse powers of the driving frequency. In this way, our results provide evidence that the magnetically induced SOC can be generated in a controllable way without involving micromotion.

The reduction of the micromotion effect opens the path for the SOC implementation in systems where the Raman coupling is difficult to apply, for example, for light atoms like lithium for which the fine-structure splitting responsible for the SOC is very small. In that case the Raman transitions inducing the SOC should be very close to the excited-state resonance in order to resolve the fine structure, which might lead to significant losses. The magnetically generated SOC does not rely on the fine-structure splitting and thus provides a method for creating the SOC for a wide range of atoms including the light ones.

II. FORMULATION**A. Hamiltonian**

We consider spinful atoms affected by a time-dependent inhomogeneous magnetic field. The atomic Hamiltonian can then be separated into a spin-independent (SI) and a spin-dependent (SD) part

$$H = H_{\text{SI}} + H_{\text{SD}}. \quad (1)$$

The former SI contribution includes operators for kinetic energy for the atomic motion in the z direction and SI potential $V_{\text{SI}}(z)$, which can represent any SI potential, such as a

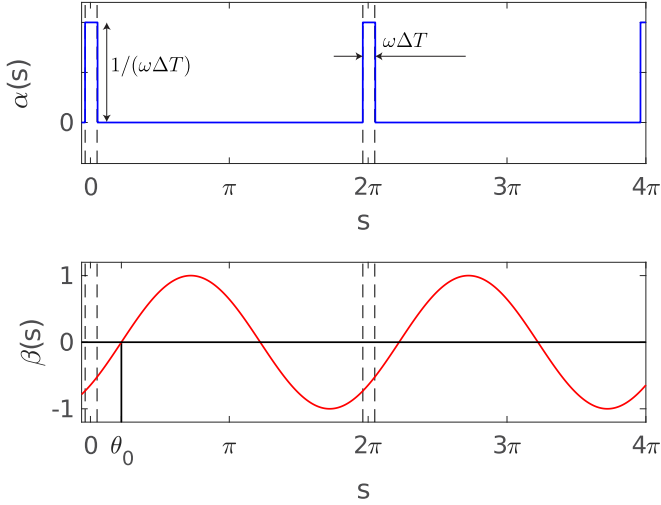


FIG. 1. Shape of the periodic functions $\alpha(s)$ and $\beta(s)$.

parabolic trap or an optical lattice

$$H_{\text{SI}} = \frac{p_z^2}{2m} + V_{\text{SI}}(z), \quad (2)$$

where z and $p_z = -i\hbar\partial_z$ are the atomic position and momentum operators, respectively, and m is the atomic mass.

On the other hand, the SD terms reads

$$H_{\text{SD}} = \omega f(t)\beta(\omega t)k_\beta z S_z + \Delta\omega_0 S_z + \omega_\alpha g(t)\alpha(\omega t)S_x, \quad (3)$$

where S_u (with $u = x, y, z$) are the Cartesian components of the spin operator \mathbf{S} . The first term in Eq. (3) represents the spin-dependent linear potential slope due to the inhomogeneous magnetic field along the z axis. It is characterized by a slowly changing dimensionless amplitude $f(t)$ and a periodic part $\beta(\omega t) = \beta(\omega t + 2\pi)$ oscillating with a frequency $\omega = 2\pi/T$. As illustrated in Fig. 1, the latter function $\beta(\omega t)$ is taken to be sinusoidal with a tunable phase θ_0 ,

$$\beta(\omega t) = \sin(\omega t - \theta_0). \quad (4)$$

The second term in Eq. (3) includes a possible detuning $\Delta\omega_0$ between the neighboring spin projection states. The third term is due to a pulsed Zeeman field oriented along the x axis. The Zeeman term is characterized by a slowly changing dimensionless amplitude $g(t)$ and a periodic part $\alpha(\omega t) = \alpha(\omega t + 2\pi)$. The latter $\alpha(\omega t)$ has large nonzero values only for a short temporal duration $\Delta T \ll T$ around multiple integers of the driving period $t = nT$ (see Fig. 1), where n is an integer, and each peak is normalized to unity,

$$\frac{1}{2\pi} \int_{-\pi}^{\pi} \alpha(s) ds = 1. \quad (5)$$

For example, $\alpha(\omega t)$ can be composed of a series of square potentials of a temporal width ΔT :

$$\alpha(\omega t) = \begin{cases} \frac{1}{\omega\Delta T}, & -\frac{\Delta T}{2} + nT \leq t < \frac{\Delta T}{2} + nT \\ 0, & \frac{\Delta T}{2} + nT \leq t < T - \frac{\Delta T}{2} + nT. \end{cases} \quad (6)$$

A specific condition regarding how short the Zeeman pulses should be is presented in Appendix A 2. In writing Eq. (3) we have introduced a wave number k_β and a Rabi frequency

ω_α characterizing the strength of the gradient and Zeeman fields, respectively. The spin-dependent Hamiltonian of the form of Eq. (3) can be simulated using a setup which involves an oscillating quadrupole magnetic, a strong bias magnetic field along the quantization axis z , and an oscillating radio-frequency magnetic field along the orthogonal (x) direction (see the Supplemental Material of Ref. [17]).

In previous studies [16,17] the gradient and Zeeman field were considered to have constant temporal profiles $f(t) = g(t) = 1$. In that case the temporal evolution of the periodically driven quantum system is sensitive to the choice of the initial and final times due to the micromotion [24–26]. To avoid the effect of micromotion, here we introduce the slowly changing amplitudes of the oscillating gradient and Zeeman fields $f(t)$ and $g(t)$ which describe a smooth switching on and off of these fields. By setting these amplitudes to zero at the initial and final times, we demonstrate that the overall dynamics of the periodically driven system is not sensitive to the specific choice of the initial and final times and is well described by the slowly changing effective Floquet Hamiltonian.

We consider the following timing of the Zeeman and the gradient magnetic fields. Initially, both fields are zero: $g(t) = f(t) = 0$ for $t \leq t_{\text{in}}$. The amplitude $f(t)$ of the gradient field is ramped up slowly from $f(t_{\text{in}}) = 0$ at the initial time t_{in} to a saturation value $f(t'_{\text{in}}) = 1$ at time $t = t'_{\text{in}}$, as illustrated schematically in Fig. 2. During the time interval $t_{\text{in}} < t < t'_{\text{in}}$ the amplitude $g(t)$ of the pulsed Zeeman field remains zero and is ramped up during the next time interval $t'_{\text{in}} < t < t''_{\text{in}}$ after the saturation of $f(t)$ is reached, as one can see in Fig. 2. The amplitudes are constant $f(t) = g(t) = 1$ for $t''_{\text{in}} < t < t'_{\text{fin}}$ and subsequently are ramped down in the opposite order. Specifically, the amplitude $g(t)$ is ramped down first at $t'_{\text{fin}} < t < t''_{\text{fin}}$ and finally the amplitude $f(t)$ goes to zero at $t'_{\text{fin}} < t < t_{\text{fin}}$, as illustrated in Fig. 2. The implications of such a timing for the ramping up and down of the periodic perturbation are discussed next.

B. Elimination of the spin-dependent potential slope

The multiplier ω in the first term of Eq. (3) reflects the fact that by increasing the driving frequency the amplitude of inhomogeneous magnetic field is also increased. On the other hand, we are interested in the high-frequency limit where the frequency of the periodic driving ω exceeds all other characteristic frequencies featured in the Hamiltonian. This is not the case for the spin-dependent potential slope $\omega f(t)\beta(\omega t)k_\beta z S_z$, so this term will be eliminated in the Hamiltonian (3) via a time-dependent unitary transformation

$$\tilde{U}_z(t) = \exp\left(-i\frac{z}{\hbar}k_\beta S_z \gamma(t)\right), \quad (7)$$

where

$$\gamma(t) = \omega \int_{t_{\text{in}}}^t f(t_1)\beta(\omega t_1) dt_1. \quad (8)$$

Here the lower integration limit is taken to be the initial time t_{in} , so that

$$\gamma(t_{\text{in}}) = 0, \quad \tilde{U}_z(t_{\text{in}}) = 1. \quad (9)$$

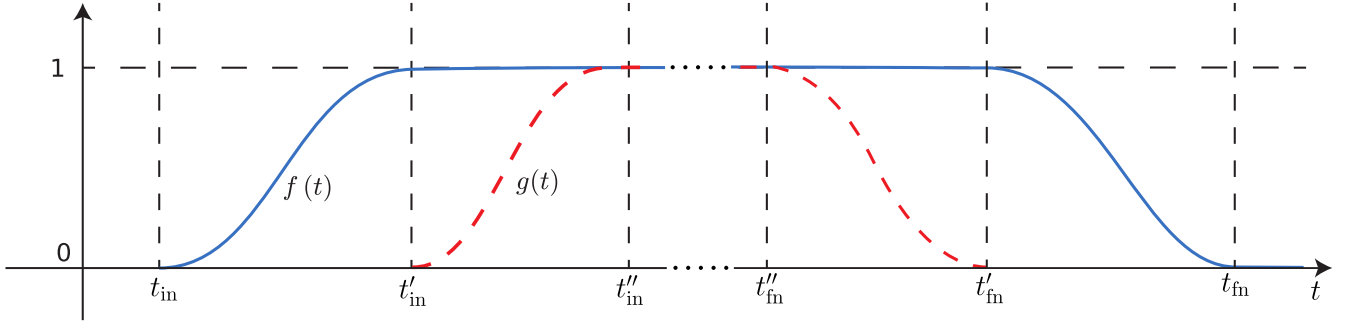


FIG. 2. Schematic representation of the switching on and off of the slowly varying amplitudes $f(t)$ and $g(t)$ of the gradient and Zeeman fields represented by blue solid and red dashed lines, respectively.

Thus the original and transformed representations coincide at the initial time $t = t_{\text{in}}$. Both representations coincide also at the final time t_{fn} provided $f(t)$ is a smooth function changing little within the driving period $T = 2\pi/\omega$. Indeed, in that case the function $\gamma(t) \equiv \gamma(\omega t, t)$ can be expanded as (see Appendix A 1)

$$\begin{aligned} \gamma(\omega t, t) &= -f(t) \cos(\omega t - \theta_0) + \frac{f'(t)}{\omega} \sin(\omega t - \theta_0) \\ &\quad + \frac{f''(t)}{\omega^2} \cos(\omega t - \theta_0) + \dots, \end{aligned} \quad (10)$$

so, using $f(t_{\text{fn}}) = f'(t_{\text{fn}}) = f''(t_{\text{fn}}) = \dots = 0$, one finds that

$$\gamma(t_{\text{fn}}) = 0, \quad \tilde{U}_z(t_{\text{fn}}) = 1. \quad (11)$$

As the amplitude $f(t)$ changes little within the driving period [$f'(t)/\omega \ll f(t)$, $f''(t)/\omega \ll f'(t)$, etc.], for the present purposes it is sufficient to keep only the zeroth-order term in Eq. (10), giving

$$\gamma(\omega t, t) \approx -f(t) \cos(\omega t - \theta_0). \quad (12)$$

The transformed Hamiltonian $\tilde{H}(t) = \tilde{U}_z^\dagger H \tilde{U}_z - i\hbar \tilde{U}_z^\dagger \partial_t \tilde{U}_z$ reads

$$\begin{aligned} \tilde{H}(\omega t, t) &= H_{\text{SI}} - \frac{p_z k_\beta}{m} S_z \gamma(\omega t, t) + \omega_\alpha g(t) \alpha(\omega t) \tilde{S}_x(z, \omega t, t) \\ &\quad + \frac{k_\beta^2}{2m} S_z^2 \gamma^2(\omega t, t), \end{aligned} \quad (13)$$

where the transformed spin operator $\tilde{S}_x(z, t) = \tilde{U}_z^\dagger S_x \tilde{U}_z$ describes spin rotation around the z axis:

$$\tilde{S}_x(z, \omega t, t) = \cos[zk_\beta \gamma(\omega t, t)] S_x - \sin[zk_\beta \gamma(\omega t, t)] S_y. \quad (14)$$

The periodic function $\alpha(\omega t)$ multiplying $\tilde{S}_x(z, t)$ in the Hamiltonian of Eq. (13) is nonzero only in a narrow vicinity of multiple integers of the driving period $T = 2\pi/\omega$. Therefore, one can replace $\gamma(t) \equiv \gamma(\omega t, t)$ by $\gamma(0, t) = -f(t) \cos \theta_0$ in Eq. (14) for $\tilde{S}_x(z, t)$ (see Appendix A 2 for estimating an error). Furthermore, since the function $f(t)$ reaches its saturation value $f(t) = 1$ when $g(t)$ is still zero, one can set $f(t) = 1$ in $\gamma(0, t)$ entering $\tilde{S}_x(z, t)$, so that one can make the following replacement in the Hamiltonian of Eq. (13):

$$\tilde{S}_x(z, \omega t, t) \rightarrow \tilde{S}_x(z, t) \quad (15)$$

with

$$\tilde{S}_x(z, t) = \cos(zk_\beta \cos \theta_0) S_x + \sin(zk_\beta \cos \theta_0) S_y. \quad (16)$$

The amount of spin rotation is thus determined by the wave number $k_\beta \cos \theta_0$ times the distance z .

III. EXACT AND EFFECTIVE EVOLUTION

A. Effective Floquet Hamiltonian

In the original Hamiltonian given by Eqs. (1)–(3) the periodic perturbation represents the spin-dependent potential slope $\omega f(t) \beta(\omega t) k_\beta z S_z$ proportional to ω . In the transformed Hamiltonian $\tilde{H}(\omega t, t)$ given by Eq. (13) this term is eliminated and the oscillating perturbation is no longer proportional to the driving frequency ω . The atomic dynamics can then be well described in terms of a slowly changing effective Floquet Hamiltonian $H_{\text{eff}}(t)$ which can be expanded in the powers of the inverse driving frequency $1/\omega$, a procedure known as the high-frequency expansion [26],

$$H_{\text{eff}}(t) = H_{\text{eff}(0)}(t) + H_{\text{eff}(1)}(t) + \dots, \quad (17)$$

where the n th term $H_{\text{eff}(n)}$ is proportional to ω^{-n} . We restrict consideration to the first two terms given by

$$H_{\text{eff}(0)} = H^{(0)}(t), \quad (18)$$

$$H_{\text{eff}(1)}(t) = \frac{1}{\hbar\omega} \sum_{l=1}^{\infty} \frac{1}{l} [H^{(l)}(t), H^{(-l)}(t)], \quad (19)$$

where $H^{(l)}(t)$ are slowly changing operators featured in the Fourier expansion of the time-periodic Hamiltonian $H(\omega t, t) = H(\omega t + 2\pi, t)$ with respect to the first argument ωt :

$$H(\omega t, t) = \sum_{l=-\infty}^{\infty} H^{(l)}(t) e^{il\omega t}. \quad (20)$$

Since $\gamma(\omega t, t)$ given by Eq. (10) is expanded in the inverse powers of ω , the Fourier components $H^{(l)}(t)$ can also be expanded in powers of $1/\omega$, i.e., $H^{(l)}(t) = H_0^{(l)}(t) + H_1^{(l)}(t) + \dots$. In the present situation $H_1^{(0)}(t) = 0$, so it is sufficient to keep only the leading term of $\gamma(\omega t, t)$ given by Eq. (12) when considering $H_{\text{eff}(0)}(t)$ and $H_{\text{eff}(1)}(t)$.

The Fourier component $H^{(0)}(t)$ providing the zeroth-order effective Floquet Hamiltonian $\tilde{H}_{\text{eff}(0)}(t)$ is obtained by averaging the Hamiltonian $\tilde{H}(\omega t, t)$ with respect to the rapidly

changing argument ωt . According to Eq. (10), the function $\gamma(\omega t, t)$ averages to zero $(2\pi)^{-1} \int_0^{2\pi} \gamma(s, t) ds = 0$ and the average of its square is $(2\pi)^{-1} \int_0^{2\pi} \gamma^2(s, t) ds = f^2(t)/2$. Furthermore, according to Eq. (5), $\alpha(\omega t)$ averages to unity over the period. Thus, using Eqs. (13) and (16) for $\tilde{H}(\omega t, t)$, the slowly changing zeroth-order effective Floquet Hamiltonian reads

$$\tilde{H}_{\text{eff}(0)}(t) = H_{\text{SI}} + \frac{g(t)\omega_\alpha}{2\pi} \tilde{S}_x(z, t) + \frac{k_\beta^2 f^2(t)}{4m} S_z^2. \quad (21)$$

In what follows we consider the case of the spin 1/2 for which the Cartesian components of the spin operator read $S_u = \hbar\sigma_u/2$ (with $u = x, y, z$), where σ_u are the Pauli matrices. In that case $S_z^2 = \hbar^2/4$, so the last term of Eq. (21) is spin independent and represents the slowly changing shift in the origin of energy. As demonstrated in Appendix B, for the spin 1/2 one can make simplifications also to the first-order effective Hamiltonian, leading to the result

$$H_{\text{eff}(1)}(t) = \frac{\omega_\alpha \hbar k_\beta f(t) g(t)}{4\pi m \hbar \omega} \sin(\theta_0) (p_z \tilde{S}_y + \tilde{S}_y p_z), \quad (22)$$

where $\tilde{S}_y \equiv \tilde{S}_y(z, t)$ is given by

$$\tilde{S}_y(z, t) = \cos(zk_\beta \cos \theta_0) S_y - \sin(zk_\beta \cos \theta_0) S_x. \quad (23)$$

Note that the first-order contribution $\tilde{H}_{\text{eff}(1)}(t)$ to the effective Hamiltonian reduces to zero for the most interesting situation where $\theta_0 = 0$, in which the momentum of spin-orbit coupling $k_\beta \cos \theta_0$ is maximum and the condition (A4) holds the best, as discussed below. In that case the zeroth-order effective Hamiltonian $\tilde{H}_{\text{eff}(0)}(t)$ describes effectively the evolution of the system up to the terms quadratic in the inverse frequency $1/\omega$.

The operators $\tilde{H}_{\text{eff}(0)}(t)$ and $\tilde{H}_{\text{eff}(1)}(t)$ change slowly in time due to slow changes of the amplitudes of the gradient and Zeeman fields $f(t)$ and $g(t)$. The spin rotation term in Eq. (21) for the effective Hamiltonian $\tilde{H}_{\text{eff}(0)}(t)$ represents the SOC characterized by the slowly changing strength $g(t)\omega_\alpha$ and the wave number of the momentum transfer $k_0 = k_\beta \cos \theta_0$. The wave number k_0 is determined by the phase θ_0 between the gradient and the pulsed Zeeman fields, like in the stationary case where $f(t) = g(t) = 1$ [17]. The momentum transfer is maximum and equals k_β for $\theta_0 = 0$ when the spikes of the infrared Zeeman field are situated at zeros of the gradient field. In that case the condition (A4) holds best and also there is no first-order contribution to the effective Hamiltonian $\tilde{H}_{\text{eff}(1)}(t) = 0$. On the other hand, the momentum transfer is zero for $\theta_0 = \pm\pi/2$ when the spikes of the Zeeman field coincide with maxima and minima of the gradient field.

B. Dynamics of the system

The overall dynamics of the state vector of the system from the initial to the final times governed by the slowly changing periodic Hamiltonian $\tilde{H}(\omega t, t) = \tilde{H}(\omega t + 2\pi, t)$ is described by the evolution operator

$$U(t_{\text{fn}}, t_{\text{in}}) = \mathcal{T} \exp\left(-\frac{i}{\hbar} \int_{t_{\text{in}}}^{t_{\text{fn}}} \tilde{H}(\omega t', t') dt'\right), \quad (24)$$

where \mathcal{T} signifies the time ordering. The operator $U(t_{\text{fn}}, t_{\text{in}})$ can be represented in terms of the effective evolution

operator $U_{\text{eff}}(t_{\text{fn}}, t_{\text{in}})$ due to the slowly changing effective Hamiltonian $\tilde{H}_{\text{eff}}(t)$ and the micromotion operators $U_{\text{micro}}(\omega t, t)$ and $U_{\text{micro}}^\dagger(\omega t, t)$ calculated at the initial and final times $t = t_{\text{in}}$ and $t = t_{\text{fn}}$ [26]:

$$U(t_{\text{fn}}, t_{\text{in}}) = U_{\text{micro}}(\omega t_{\text{fn}}, t_{\text{fn}}) U_{\text{eff}}(t_{\text{fn}}, t_{\text{in}}) U_{\text{micro}}^\dagger(\omega t_{\text{in}}, t_{\text{in}}). \quad (25)$$

Here the effective evolution is given by

$$U_{\text{eff}}(t_{\text{fn}}, t_{\text{in}}) = \mathcal{T} \exp\left(-\frac{i}{\hbar} \int_{t_{\text{in}}}^{t_{\text{fn}}} \tilde{H}_{\text{eff}}(t') dt'\right) \quad (26)$$

and the micromotion operator reads, up to the terms linear in $1/\omega$,

$$U_{\text{micro}}(\omega t, t) \approx 1 - \frac{1}{\hbar\omega} \sum_{m \neq 0} \frac{1}{m} H^{(m)}(t) e^{im\omega t}. \quad (27)$$

The operator $U_{\text{micro}}(\omega t, t)$ describes effects due to the fast changes of the Hamiltonian $\tilde{H}(\omega t, t)$. It goes to the unity when periodic driving switches off [26]. Thus, in the present situation the micromotion operator $U_{\text{micro}}(\omega t, t)$ reduces to unity for $t = t_{\text{in}}$ and $t = t_{\text{fn}}$. In this way, the overall dynamics described by the slowly changing effective Floquet Hamiltonian $\tilde{H}_{\text{eff}}(t) = \tilde{H}_{\text{eff}(0)}(t) + \tilde{H}_{\text{eff}(1)}(t) + \dots$ should reproduce well the exact dynamics governed by the exact Hamiltonian $\tilde{H}(\omega t, t)$. An additional temporal dependence is due to the time-dependent unitary operator $\tilde{U}_z(t)$ transforming the original state vector to the new representation. However, the transformation $\tilde{U}_z(t)$ given by Eq. (7) reduces to unity at the initial and final times and thus does not affect the overall evolution of the system from the initial to the final times. Therefore, one can consider the time evolution from the initial to the final times governed by the transformed Hamiltonian $\tilde{H}(\omega t, t)$, which in turn can be described by the slowly changing effective Floquet Hamiltonian $\tilde{H}_{\text{eff}}(t)$, i.e.,

$$U(t_{\text{fn}}, t_{\text{in}}) = U_{\text{eff}}(t_{\text{fn}}, t_{\text{in}}). \quad (28)$$

In the next section we make sure that this is the case.

In the stationary regime where $f(t) = g(t) = 1$ the effective Floquet Hamiltonian (21) becomes time independent and for the case of spin 1/2 is given by

$$\tilde{H}_{\text{eff}(0)} = H_{\text{SI}} + \frac{\omega_\alpha}{2\pi} [\cos(zk_0) S_x - \sin(zk_0) S_y] + \frac{\hbar^2 k_\beta^2}{16m}, \quad (29)$$

with $k_0 = k_\beta \cos \theta_0$. The effective Hamiltonian given by Eq. (21) or (29) is analogous to the light-induced coupling between the (quasi-)spin-up and -down states accompanied by the recoil k_0 , like the one used to study the spin squeezing in optical lattices [13]. The Hamiltonian reduces to the SOC involving coupling between the linear momentum p_x and the spin component S_x via the unitary transformation $\exp(i\frac{z}{\hbar} k_0 S_z)$ [5]. Note also that the effective Hamiltonian (21) or (29) has been derived under the high-frequency assumption, implying that the driving frequency is larger than all the frequencies associated with the time-periodic Hamiltonian $\tilde{H}(\omega t, t)$ changing slowly within the driving period. In that case the effective Hamiltonian reproduces very well the exact evolution, as we will see next.

C. Exact vs numerical results

We compare the time evolution of the time-dependent Schrödinger equation, calculated numerically for both cases: the exact time-periodic Hamiltonian $\tilde{H}(\omega t, t)$ and the effective Hamiltonian $\tilde{H}_{\text{eff}(0)}(t)$. The two-component (spinor) wave functions $|\psi(t)\rangle$ and $|\phi(t)\rangle$ governed by $\tilde{H}(\omega t, t)$ and $\tilde{H}_{\text{eff}(0)}(t)$, respectively, are chosen to be the same at the initial time $|\phi(t_{\text{in}})\rangle = |\psi(t_{\text{in}})\rangle$. Both spinor wave functions should be almost identical at the final time $|\phi(t_{\text{fin}})\rangle = |\psi(t_{\text{fin}})\rangle$ if the high-frequency conditions are met: (i) $p_z^2/2m \ll \hbar\omega$, (ii) $p_z k_0/m \ll \omega$, (iii) $\omega_\alpha \ll \omega$, and (iv) $f'(t) \ll \omega$ and $g'(t) \ll \omega$. Additionally, the duration of the Zeeman pulses ΔT should be small enough compared to the driving period $T = 2\pi/\omega$, so there is an extra condition following from (A4) in Appendix A 2: (v) $Lk_\beta|\omega\Delta T \sin\theta_0 - [(\omega\Delta T)^2/2] \cos\theta_0| \ll 1$, where the sample length L is taken to be much larger than the inverse momentum $1/k_\beta$, i.e., $Lk_\beta \gg 1$. Condition (v) is satisfied in the experiment [17] where the sample length is of the order of $100 \mu\text{m}$, the wave number k_β is of the order of $(\mu\text{m})^{-1}$, and $\omega\Delta T = 0.01 \ll 1$. Note that condition (v) holds best if the phase difference is zero $\theta_0 = 0$, i.e., when the spikes of the Zeeman field $\alpha(\omega t)$ are situated at zero points of the profile $\beta(\omega t)$. In that case condition (v) reduces to $Lk_\beta(\omega\Delta T)^2/2 \ll 1$.

In the numerical calculations, we assume that the atoms are confined in a square well with infinitely high potential boundaries at $z = \pm L/2$ and zero potential for $z \in [-L/2, L/2]$. The ramping functions $f(t)$ and $g(t)$ are taken to have the form

$$f(t) = \frac{1}{2} \{ \tanh[c(t - \tau/2)] + \tanh[c(7\tau/2 + \tau'' - t)] \}, \quad (30)$$

$$g(t) = \frac{1}{2} \{ \tanh[c(t - 3\tau/2)] + \tanh[c(5\tau/2 + \tau'' - t)] \}, \quad (31)$$

where τ'' is the time interval between the ramping on and off, $1/c$ is the ramping time of the periodic driving, and τ is the time delay between the ramping of the functions $f(t)$ and $g(t)$. By taking $c\tau > 4$ we choose $t_{\text{in}} = 0$, $t'_{\text{in}} = \tau$, and $t''_{\text{in}} = 2\tau$ and similarly $t'_{\text{fin}} = \tau'' + 2\tau$, $t''_{\text{fin}} = \tau'' + 3\tau$, and $t_{\text{fin}} = \tau'' + 4\tau$. In that case we have $f(0) \approx g(\tau) \approx 0$ and $f(\tau) \approx g(2\tau) \approx 1$, as well as $f(\tau'' + 4\tau) \approx g(\tau'' + 3\tau) \approx 0$ and $f(\tau'' + 3\tau) \approx g(\tau'' + 2\tau) \approx 1$, as illustrated in Fig. 2.

Note that, according to condition (iv) presented at the beginning of Sec. III C, the ramping rate $f'(t) \sim c$ should be much smaller than the driving frequency ω . On the other hand, the ramping time should be smaller than the decoherence time τ_{decoh} . The latter condition cannot be met in the experiment of Ref. [17] in which the decoherence time is of the order of 1 ms whereas the driving period is only around 10 times smaller. To satisfy the slow ramping condition, one should increase the decoherence time, which is expected to be done in the future experiments. In the subsequent plots displayed in Figs. 3 and 4 the ramping rate is taken to be 100 times smaller than the driving frequency, which can be applied to future experiment with the relative decoherence times $\omega\tau_{\text{decoh}}$ larger than that in Ref. [17].

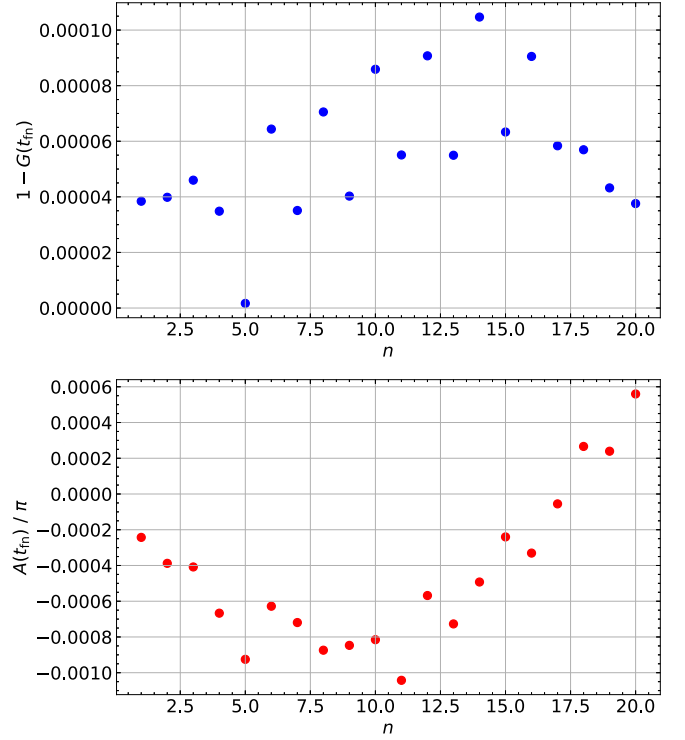


FIG. 3. Functions $G(t_{\text{in}})$ and $A(t_{\text{in}})$ involving three different polarizations $i \in \{x, y, z\}$ for the following parameters: $\omega = 100E_{\text{R}}$, $\omega_\alpha = E_{\text{R}}$, $c = k_{\text{R}}$, $\tau = 5E_{\text{R}}^{-1}$, $\tau'' = 5E_{\text{R}}^{-1}$, $\omega\Delta T = 0.01$, $\theta_0 = 0$, $k_\beta = k_{\text{R}}$, and $L = 100k_{\text{R}}^{-1}$.

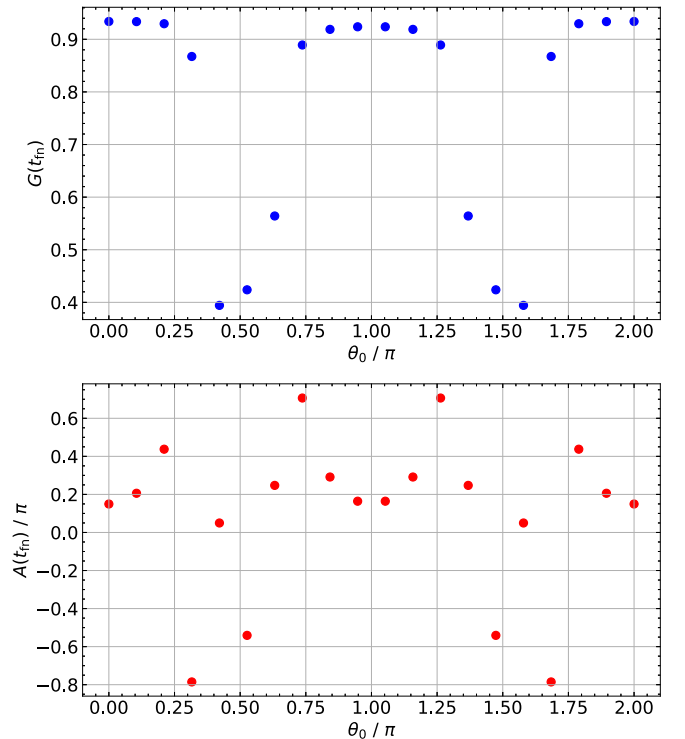


FIG. 4. Comparison of dependence of functions $G(t_{\text{in}})$ and $A(t_{\text{in}})$ on θ_0 for the following parameters: $\omega = 10E_{\text{R}}$, $\omega_\alpha = E_{\text{R}}$, $c = 0.1E_{\text{R}}$, $\tau = 100E_{\text{R}}^{-1}$, $\tau'' = 150E_{\text{R}}^{-1}$, $\omega\Delta T = 0.01$, $n = 1$, $k_\beta = k_{\text{R}}$, and $L = 100k_{\text{R}}^{-1}$.

1. Comparison of exact and effective dynamics

To compare the dynamics, we look at the inner product between the state vectors $|\phi(t)\rangle$ and $|\psi(t)\rangle$ evolving by the exact time-periodic Hamiltonian $\tilde{H}(\omega t, t)$ and the effective slowly changing Hamiltonian $\tilde{H}_{\text{eff}(0)}(t)$, respectively,

$$\begin{aligned} \langle \psi(t) | \phi(t) \rangle &= \int_0^L dz \langle \psi(t, z) | \phi(t, z) \rangle \\ &= \int_0^L dz \sum_{s=\{\uparrow, \downarrow\}} \langle \psi(t, z) | s \rangle \langle s | \phi(t, z) \rangle. \end{aligned} \quad (32)$$

If the inner product $\langle \psi(t) | \phi(t) \rangle$ is unity for $t = t_{\text{fin}}$, the overall dynamics of the two state vectors is equivalent. Otherwise, this is not the case. Thus, for numerics, one may look at $|\langle \psi(t) | \phi(t) \rangle|$ and $\arg[\langle \psi(t) | \phi(t) \rangle]$. Deviations of these quantities from 1 and 0, respectively, signify differences between the state vectors and thus the nonequivalence of the dynamics. We explore these differences for state vectors characterized by three orthogonal initial spin polarizations. For this we introduce the functions

$$G(t) := \frac{1}{3} \sum_{i=\{x,y,z\}} |\langle \psi^{(i)}(t) | \phi^{(i)}(t) \rangle|, \quad (33)$$

$$A(t) := \frac{1}{3} \sum_{i=\{x,y,z\}} \arg \langle \psi^{(i)}(t) | \phi^{(i)}(t) \rangle, \quad (34)$$

where once again deviations of these functions from 1 and 0 signify differences between the state vectors. Specifically, the spatial part of the initial state vectors is taken to be an eigenstate of the box potential $\Phi_n(z)$ and the spin is pointing along the x , y , and z axis,

$$|\psi_n^{(i)}(t=0)\rangle = \Phi_n(z) |i\rangle, \quad i \in \{x, y, z\}, \quad (35)$$

where

$$\Phi_n(z) = \sqrt{\frac{2}{L}} \sin\left(\frac{\pi n}{L} z\right) \quad (36)$$

and

$$|x\rangle = \frac{1}{\sqrt{2}} \begin{pmatrix} 1 \\ 1 \end{pmatrix}, \quad |y\rangle = \frac{1}{\sqrt{2}} \begin{pmatrix} 1 \\ i \end{pmatrix}, \quad |z\rangle = \begin{pmatrix} 1 \\ 0 \end{pmatrix}. \quad (37)$$

The functions $G(t_{\text{fin}})$ and $A(t_{\text{fin}})$ are presented in Fig. 3. One can see that $G(t_{\text{fin}}) \approx 1$ and $A(t_{\text{fin}}) \approx 0$. This shows that for $\theta = 0$ the overall dynamics from the initial to the final times is well described in terms of the effective dynamics governed by the zeroth-order effective Hamiltonian. Indeed, the first-order effective Hamiltonian $\tilde{H}_{\text{eff}(1)}(t)$ presented in Eq. (22) goes to zero for $\theta_0 = \pi n_0$, where n_0 is an integer number. Additionally, due to adiabatic ramping described by the ramping functions $f(t)$ and $g(t)$, the effects of micromotion disappear at the initial and final times in the plots displayed in Fig. 3 as well as in Fig. 4. Therefore, for $\theta_0 = \pi n_0$, the approximate dynamics given by the zeroth-order effective Hamiltonian $\tilde{H}_{\text{eff}(0)}(t)$ is accurate up to second order in the inverse frequency.

2. First-order correction effect

If $\theta_0 \neq \pi n_0$, the first-order effective Hamiltonian is no longer zero and the approximate dynamics is accurate only

up to first order in the inverse frequency. In Fig. 4 we demonstrate the difference in the approximation accuracy for various θ_0 by calculating the dependence of $G(t_{\text{fin}})$ on θ_0 . One can see clearly that the approximation holds best for $\theta_0 \approx \pi n_0$, for which $\tilde{H}_{\text{eff}(1)} = 0$. Here we have deliberately chosen the driving frequency ω to be considerably smaller than the one used in other plots so that one can more clearly see the relative importance of first-order correction term $\tilde{H}_{\text{eff}(1)}$.

IV. CONCLUSION

We have demonstrated how to bypass the micromotion emerging in the magnetically induced SOC by switching on and off in a proper way the oscillating magnetic fields at the initial and final times. We have studied the exact dynamics of the system from the initial to the final times governed by the time-periodic Hamiltonian and compared it to the dynamics described by the slowly changing effective Floquet Hamiltonian. The two dynamics agree well under the assumption of the high-frequency driving. The agreement is shown to be best when the phase of the periodic driving takes a specific value for which the effect of the spin-orbit coupling is maximum. In that case the first-order effective Floquet vanishes and the zeroth-order Floquet Hamiltonian is correct up to the second-order expansion in the inverse powers of the driving frequency. The overall dynamics is thus well described by the slowly changing zeroth-order effective Floquet Hamiltonian containing the SOC term. In this way, the magnetically induced SOC can be induced in a controllable way without involving the micromotion. This opens the path for practical applications of magnetically generated SOC, e.g., generation of nontrivial topological or spin-squeezed states for ultracold atoms in optical lattices, when the optically generated SOC is complicated to apply.

ACKNOWLEDGMENTS

This work was supported by the European Social Fund (Project No. 09.3.3-LMT-K-712-23-0035) under a grant agreement with the Research Council of Lithuania (M.M.S.).

APPENDIX A: ANALYSIS OF $\gamma(t) = \gamma(\omega t, t)$

1. Function $\gamma(\omega t, t)$

Let us now determine how to separate a fast periodic time dependence of $\gamma(t) = \gamma(\omega t, t)$ from its additional slow temporal dependence. To that end, we expand $\gamma(t)$ as a series of $f^{(n)}(t)/\omega^n$ terms, where $f^{(n)}(t)$ denotes an n th-order temporal derivative of the slowly varying envelope function $f(t)$. Substituting Eq. (4) into (7) and integrating by parts, one finds

$$\begin{aligned} \gamma(t) &= \omega \int_{t_{\text{in}}}^t f(s) \sin(\omega s - \theta_0) ds \\ &= -f(s) \cos(\omega s - \theta_0) \Big|_{t_{\text{in}}}^t + \frac{f'(s)}{\omega} \sin(\omega s - \theta_0) \Big|_{t_{\text{in}}}^t \\ &\quad - \int_{t_{\text{in}}}^t \frac{f''(s)}{\omega} \sin(\omega s - \theta_0) ds. \end{aligned} \quad (A1)$$

This provides an expansion in a series of terms proportional to $f^{(n)}/\omega^n$,

$$\begin{aligned} \gamma(t) = \gamma(\omega t, t) = & -f(t) \cos(\omega t - \theta_0) \\ & + \frac{f'(t)}{\omega} \sin(\omega t - \theta_0) \\ & + \frac{f''(t)}{\omega^2} \cos(\omega t - \theta_0) + \dots, \end{aligned} \quad (\text{A2})$$

where we used the fact that $f(t_{\text{in}}) = f'(t_{\text{in}}) = f''(t_{\text{in}}) = 0$.

2. Estimation of error

To estimate an error made in writing Eq. (16) for $\tilde{S}_x(z, t)$, let us expand the function $\gamma(\omega t, t)$ given by Eq. (10) in the powers of $t - t_n$ around a spike centered at $t_n = nT$, with n an integer. Since the amplitude $f(t)$ reaches its stationary value when $g(t)$ is still zero, one finds, up to the quadratic term by setting $f(t) = 1$.

$$\gamma(\omega t, t) \approx -\omega(t - t_n) \sin \theta_0 + \omega^2(t - t_n)^2 \cos \theta_0. \quad (\text{A3})$$

Therefore, the maximum displacement $|t - t'_n| = \Delta T/2$ at which $\alpha(\omega t)$ is still nonzero yields the following maximum value of $|\gamma(\omega t)|$:

$$\gamma_{\text{max}} \approx |(\omega \Delta T/2) \sin \theta_0| + |(\omega \Delta T)^2/2 \cos \theta_0|. \quad (\text{A4})$$

Since $\omega \Delta T = 2\pi \Delta T/T \ll 1$, then $\gamma_{\text{max}} \ll 1$.

Equation (16) is valid if

$$Lk_\beta \gamma_{\text{max}} \ll 1, \quad (\text{A5})$$

where $L = z_{\text{max}}$ is a characteristic size of the atomic cloud. The condition (A5) holds best if the phase difference is zero $\theta_0 = 0$, i.e., when the spikes of the Zeeman field $\alpha(\omega t)$ are situated at zero points of the profile $\beta(\omega t)$. In that case $\gamma_{\text{max}} = (\omega \Delta T)^2/2$ is quadratic in $\omega \Delta T$ and the condition (A5) reduces to

$$Lk_\beta (\omega \Delta T)^2/2 \ll 1. \quad (\text{A6})$$

Equations (A4)–(A6) provide restrictions on the size of the atomic cloud L . Since $Lk_\beta \gg 1$, the width of the spikes should be sufficiently small compared to the driving period $T = 2\pi/\omega$.

APPENDIX B: FIRST-ORDER EFFECTIVE HAMILTONIAN

Here we provide explicit calculations of the first-order effective Hamiltonian in the transformed frame. The general formula for the first-order effective Hamiltonian is presented by Eq. (22),

$$\tilde{H}_{\text{eff}(1)}(t) = \frac{1}{\hbar\omega} \sum_{l=1}^{\infty} \frac{1}{l} [\tilde{H}^{(l)}(t), \tilde{H}^{(-l)}(t)], \quad (\text{B1})$$

where $\tilde{H}^{(l)}(t)$ are the Fourier components of the transformed Hamiltonian $\tilde{H}(\omega t, t)$ with respect to the first argument ωt . The latter $\tilde{H}(\omega t, t)$ is given by Eq. (13),

$$\begin{aligned} \tilde{H}(\omega t, t) = & H_{\text{SI}} - \frac{p_z k_\beta}{m} S_z \gamma(\omega t, t) \\ & + \omega_\alpha g(t) \alpha(\omega t) \tilde{S}_x(z, t) + \frac{k_\beta^2}{2m} \gamma^2(\omega t, t) S_z^2. \end{aligned} \quad (\text{B2})$$

Using the approximate expression (12) for $\gamma(\omega t, t)$, one has $\gamma(\omega t, t) \approx -f(t) \cos(\omega t - \theta_0)$. Thus the nonzero Fourier modes of $\gamma(\omega t, t)$ with $m = \pm 1$ read

$$\gamma^{(\pm 1)}(t) = -\frac{f(t)}{2} e^{\mp i\theta_0}. \quad (\text{B3})$$

Since the amplitude $\alpha(\omega t)$ is composed of sharp peaks at $t = nT$, the Fourier components $\alpha^{(\pm l)}$ weakly depend on l and can be written $\alpha^{(\pm l)} = 1/2\pi$ for any $l \geq 0$.

Next we analyze the specific Fourier components $H^{(\pm l)}$ contributing to the effective Hamiltonian (B1).

1. Contribution by $l = 1$ Fourier modes

Fourier components $\tilde{H}^{(l)}$ with $l = \pm 1$ are

$$\tilde{H}^{(\pm 1)}(t) = \frac{k_\beta f(t)}{2m} e^{\mp i\theta_0} p_z S_z + \frac{\omega_\alpha g(t)}{2\pi} \tilde{S}_x. \quad (\text{B4})$$

The corresponding commutator featured in the effective Hamiltonian (B1) reads

$$[\tilde{H}^{(1)}, \tilde{H}^{(-1)}] = -\frac{i\omega_\alpha k_\beta f(t) g(t)}{2\pi m} \sin(\theta_0) [p_z S_z, \tilde{S}_x]. \quad (\text{B5})$$

The commutator may be rewritten as

$$[p_z S_z, \tilde{S}_x] = p_z [S_z, \tilde{S}_x] + [p_z, \tilde{S}_x] S_z, \quad (\text{B6})$$

where

$$\tilde{S}_x(z, t) = \cos(zk_\beta \cos \theta_0) S_x + \sin(zk_\beta \cos \theta_0) S_y. \quad (\text{B7})$$

Using $[S_z, \tilde{S}_x] = i\hbar \tilde{S}_y$ and $[p_z, \tilde{S}_x] = -i\hbar k_\beta \cos \theta_0 \tilde{S}_y$, one obtains

$$[p_z S_z, \tilde{S}_x] = i\hbar p_z \tilde{S}_y - i\hbar k_\beta \cos \theta_0 \tilde{S}_y S_z, \quad (\text{B8})$$

where

$$\tilde{S}_y = \cos(zk_\beta \cos \theta_0) S_y - \sin(zk_\beta \cos \theta_0) S_x. \quad (\text{B9})$$

In what follows we will consider the case of the spin 1/2. In that case one has $\tilde{S}_y S_z = i\hbar \tilde{S}_x/2$, so one can make further simplifications using $i\hbar k_\beta \cos \theta_0 \tilde{S}_x = [p_z, \tilde{S}_y]$. Consequently, the commutator featured in Eq. (B5) reduces to

$$[p_z S_z, \tilde{S}_x] = i\frac{\hbar}{2} (p_z \tilde{S}_y + \tilde{S}_y p_z). \quad (\text{B10})$$

Substituting Eq. (B10) into Eqs. (B5) and (B1), one arrives at the first-order effective Hamiltonian given by Eq. (22).

2. Contribution by $l = 2$ Fourier modes

Noting that

$$\gamma^2(\omega t, t) \approx \frac{f^2(t)}{2} \left(1 - \frac{1}{2} e^{-i2\theta_0} e^{i2\omega t} - \frac{1}{2} e^{i2\theta_0} e^{-i2\omega t} \right), \quad (\text{B11})$$

the Fourier modes $\tilde{H}^{(l)}$ with $l = \pm 2$ read

$$\tilde{H}^{(\pm 2)}(t) = \frac{\omega_\alpha g(t)}{2\pi} \tilde{S}_x - \frac{k_\beta^2 f^2(t)}{32m} e^{\mp i2\theta_0} S_z^2. \quad (\text{B12})$$

For spin 1/2 one has $S_z^2 = 1/4$, so the last term of Eq. (B12) is proportional to the identity operator and the commutator $[\tilde{H}^{(2)}(t), \tilde{H}^{(-2)}(t)]$ reduces to zero. For arbitrary spin, the

commutator $[\tilde{H}^{(2)}(t), \tilde{H}^{(-2)}(t)]$ is no longer zero and the first-order effective Hamiltonian becomes more complicated.

3. Contribution by Fourier modes with $l > 2$

The Fourier modes $H^{(\pm l)}(t)$ with $l > 2$ are all the same:

$$H^{(\pm l)}(t) = \frac{\omega_\alpha g(t)}{2\pi} \tilde{\mathcal{S}}_x \quad \text{for } l > 2. \quad (\text{B13})$$

So the commutators $[H^{(l)}(t), H^{(-l)}(t)]$ vanish for $l > 2$.

4. Final result

In this way the first-order effective Hamiltonian reads, using Eqs. (B1), (B5), and (B10),

$$H_{\text{eff}(1)}(t) = \frac{\omega_\alpha \hbar k_\beta f(t) g(t)}{4\pi m \hbar \omega} \sin(\theta_0) (p_z \tilde{\mathcal{S}}_y + \tilde{\mathcal{S}}_y p_z). \quad (\text{B14})$$

-
- [1] R. Winkler, *Spin-Orbit Coupling Effects in Two-Dimensional Electron and Hole Systems* (Springer, Berlin, 2003).
- [2] J. Ruseckas, G. Juzeliūnas, P. Öhberg, and M. Fleischhauer, *Phys. Rev. Lett.* **95**, 010404 (2005).
- [3] T. D. Stanescu, C. Zhang, and V. Galitski, *Phys. Rev. Lett.* **99**, 110403 (2007).
- [4] G. Juzeliūnas, J. Ruseckas, M. Lindberg, L. Santos, and P. Öhberg, *Phys. Rev. A* **77**, 011802(R) (2008).
- [5] Y.-J. Lin, K. Jiménez-García, and I. B. Spielman, *Nature (London)* **471**, 83 (2011).
- [6] N. Goldman, G. Juzeliūnas, P. Öhberg, and I. B. Spielman, *Rep. Prog. Phys.* **77**, 126401 (2014).
- [7] H. Zhai, *Rep. Prog. Phys.* **78**, 026001 (2015).
- [8] V. Galitski, G. Juzeliūnas, and I. B. Spielman, *Phys. Today* **72** (1), 38 (2019).
- [9] D. Burba, H. Dunikowski, M. R. de Saint-Vincent, E. Witkowska, and G. Juzeliūnas, [arXiv:2404.12429](https://arxiv.org/abs/2404.12429).
- [10] J. Y. Vaishnav, J. Ruseckas, C. W. Clark, and G. Juzeliūnas, *Phys. Rev. Lett.* **101**, 265302 (2008).
- [11] C. S. Madasu, M. Hasan, K. D. Rathod, C. C. Kwong, and D. Wilkowski, *Phys. Rev. Res.* **4**, 033180 (2022).
- [12] M. Mamaev, I. Kimchi, R. M. Nandkishore, and A. M. Rey, *Phys. Rev. Res.* **3**, 013178 (2021).
- [13] T. Hernández Yanes, M. Płodzień, M. Mackoīt Sinkevičienė, G. Žlabys, G. Juzeliūnas, and E. Witkowska, *Phys. Rev. Lett.* **129**, 090403 (2022).
- [14] B. M. Anderson, I. B. Spielman, and G. Juzeliūnas, *Phys. Rev. Lett.* **111**, 125301 (2013).
- [15] Z.-F. Xu, L. You, and M. Ueda, *Phys. Rev. A* **87**, 063634 (2013).
- [16] X. Luo, L. Wu, J. Chen, Q. Guan, K. Gao, Z.-F. Xu, L. You, and R. Wang, *Sci. Rep.* **6**, 18983 (2016).
- [17] B. Shteynas, J. Lee, F. C. Top, J.-R. Li, A. O. Jamison, G. Juzeliūnas, and W. Ketterle, *Phys. Rev. Lett.* **123**, 033203 (2019).
- [18] M. Atala, M. Aidelsburger, M. Lohse, J. T. Barreiro, B. Paredes, and I. Bloch, *Nat. Phys.* **10**, 588 (2014).
- [19] M. Mamaev, T. Bilitewski, B. Sundar, and A. M. Rey, *PRX Quantum* **3**, 030328 (2022).
- [20] R. P. Anderson, D. Trypogeorgos, A. Valdés-Curiel, Q.-Y. Liang, J. Tao, M. Zhao, T. Andrijauskas, G. Juzeliūnas, and I. B. Spielman, *Phys. Rev. Res.* **2**, 013149 (2020).
- [21] D. Burba, M. Račiūnas, I. B. Spielman, and G. Juzeliūnas, *Phys. Rev. A* **107**, 023309 (2023).
- [22] T. Hernández Yanes, G. Žlabys, M. Płodzień, D. Burba, M. M. Sinkevičienė, E. Witkowska, and G. Juzeliūnas, *Phys. Rev. B* **108**, 104301 (2023).
- [23] M. Płodzień, M. Lewenstein, E. Witkowska, and J. Chwedeńczuk, *Phys. Rev. Lett.* **129**, 250402 (2022).
- [24] N. Goldman and J. Dalibard, *Phys. Rev. X* **4**, 031027 (2014).
- [25] A. Eckardt and E. Anisimovas, *New J. Phys.* **17**, 093039 (2015).
- [26] V. Novičenko, E. Anisimovas, and G. Juzeliūnas, *Phys. Rev. A* **95**, 023615 (2017).